LUT University

Accelerated Fe3+/Fe2+ cycle using atomic H* on Pd/Al2O3: A novel mechanism for an electrochemical system with particle electrode for iron sludge reduction in the Fe2+/peroxydisulfate oxidation process

Zeng Huabin, Zhao Xu, Zhao Feiping, Park Yuri, Sillanpää Mika

This is a Post-print version of a publication

published by Elsevier

in Chemical Engineering Journal

DOI: 10.1016/j.cej.2019.122972

Copyright of the original publication: © Elsevier 2019

Please cite the publication as follows:

Zeng, H., Zhao, X., Zhao, F., Park, Y., Sillanpää, M. (2020). Accelerated Fe3+/Fe2+ cycle using atomic H* on Pd/Al2O3: A novel mechanism for an electrochemical system with particle electrode for iron sludge reduction in the Fe2+/peroxydisulfate oxidation process. Chemical Engineering Journal, vol. 382. DOI: 10.1016/j.cej.2019.122972

This is a parallel published version of an original publication. This version can differ from the original published article.

Accelerated Fe^{3+}/Fe^{2+} Cycle using Atomic H* on Pd/Al_2O_3: A Novel Mechanism for an Electrochemical System with Particle Electrode for Iron Sludge Reduction in the Fe^{2+}/Peroxydisulfate Oxidation Process

Huabin Zeng [a*], Xu Zhao [b], Feiping Zhao [a], Yuri Park [a], Mika Sillanpää [a]

[a] Department of Green Chemistry, School of Engineering Science, Lappeenranta-Lahti University of Technology LUT, Sammonkatu 12, FI-50130 Mikkeli, Finland

[b] State Key Laboratory of Environmental Aquatic Chemistry, Research Center for Eco-Environmental Sciences, Chinese Academy of Sciences, Beijing 100085, China

*Corresponding author:

Department of Green Chemistry

LUT University

Sammonkatu 12, FI-50130 Mikkeli, Finland

E-mail address: Huabin.zeng@lut.fi

Abbreviations

BA	Benzoic acid
PDS	Peroxydisulfate
Fe^{2+}/PDS process	PDS oxidation process activated by Fe^{2+}
Fe^{3+}/PDS process	PDS oxidation process activated by Fe^{3+}
Electro/Fe^{3+}/PDS	PDS oxidation with addition of Fe^{3+} and applying current
Pd/Fe^{3+}/PDS	PDS oxidation process with the addition of Fe^{3+} and Pd/Al_2O_3 catalyst
Electro/Pd/PDS	PDS oxidation process with the addition of the Pd/Al_2O_3 catalyst and applying current
Electro/Pd/Fe^{3+}	Fe^{3+} oxidation process with the addition of the Pd/Al_2O_3 catalyst and applying current
Pd-EFP system	Pd/Al_2O_3-enhanced electro/ Fe^{3+}/PDS oxidation process
XRD	X-ray diffraction
AOPs	Advanced oxidation processes
3D	Three-dimensional
ESR	Electron spin resonance
ICP-OES	Inductively coupled plasma-optical emission spectroscopy
TBA	Tert-butyl alcohol
H_2/Pd/PDS	PDS oxidation process with the addition of the Pd/Al_2O_3 catalyst in an atmosphere of H_2

Abstract

The high cost associated with the disposal of iron sludge in Fe^{2+} activated oxidation systems significantly limits their widespread use. In this study, we constructed a trace iron-based peroxydisulfate (PDS) oxidation system (Pd-EFP) using Pd/Al_2O_3 as the particle electrode and externally added PDS as an oxidant. At an initial solution pH of 3.0 and a current density of 3.33 mA/cm^2, with the addition of 10 mM PDS, 50 mg Pd/Al_2O_3, and 2 mg/L Fe ions, 80.12% of 180 μM benzoic acid (BA) was degraded within 120 min. The Pd/Al_2O_3 catalyst provided sufficiently large surface area for atomic H* production from the adsorption of electrogenerated H_2 or H^+ conversion via electro-induction on the Pd/Al_2O_3 surface, which subsequently accelerated the transformation from Fe^{3+} to Fe^{2+}. Using this method, organics could be degraded by both $SO_4^{\cdot-}$ and ·OH via the Fe^{2+}-activated PDS process. In the Pd-EFP process, the optimal dosage of Fe ions was determined to be 36 μM (2 mg/L). Correspondently, the optimal current density and PDS concentration in the Pd-EFP system were 3.33 mA/cm^2 and 20 mM, respectively. Furthermore, degradation of BA was efficiently promoted by the N_2 atmosphere, which could steer the reaction on the surface of Pd/Al_2O_3 in the right direction toward Fe^{3+} reduction by atomic H*, by dispelling accumulated H_2 above the reaction liquid and suppressing oxygen reduction. Finally, the Pd/Al_2O_3 catalyst was found to be durable in the Pd-EFP system according to reusability experiments and X-ray diffraction patterns of the fresh and used Pd/Al_2O_3 catalyst. This research provides an environmentally benign system for recycling Fe^{3+} in Fe^{2+}/PDS processes and for suppressing iron sludge production.

Keywords: Fe^{2+}/PDS process, Pd/Al_2O_3, atomic H*, iron cycle, iron sludge reduction

1. Introduction

By producing strongly oxidising ·OH, advanced oxidation processes (AOPs) are appealing treatment options for removing non-biodegradable, recalcitrant and toxic organic contaminants from water [1-4]. Among AOPs, the Fenton reaction (**reaction 1**) has been widely applied in wastewater treatments for its high oxidation ability, low operating cost, and controllability [5]. In parallel to the Fenton reaction, the reaction between Fe^{2+} and peroxydisulfate (PDS, $S_2O_8^{2-}$) (Fe^{2+}/PDS reaction, **reaction 2**) shares similar advantages with the Fenton reaction while sulfate radical ($SO_4^{\cdot-}$) demonstrate a longer lifetime than hydroxyl radical (·OH) in water [6-8].

$$Fe^{2+} + H_2O_2 \rightarrow Fe^{3+} + \cdot OH + OH^- \quad (1)\ [9]$$

$$Fe^{2+} + S_2O_8^{2-} \rightarrow Fe^{3+} + SO_4^{\cdot-} + SO_4^{2-} \quad (2)\ [10]$$

$$S_2O_8^{2-} + SO_4^{\cdot-} \rightarrow S_2O_8^{\cdot-} + SO_4^{2-} \quad (3)\ [11]$$

$$Fe^{3+} + S_2O_8^{2-} \rightarrow Fe^{2+} + S_2O_8^{\cdot-} \quad (4)\ [12]$$

$$2S_2O_8^{2-} + 2H_2O \rightarrow 3SO_4^{2-} + SO_4^{\cdot-} + O_2^{\cdot-} + 4\ H^+ \quad (5)\ [13]$$

$$S_2O_8^{2-} + 2H_2O \rightarrow 2SO_4^{2-} + HO_2^- + 4\ H^+ \quad (6)\ [13]$$

$$Fe^{3+} + O_2^{\cdot} \rightarrow Fe^{2+} + O_2 \quad (7)\ [14]$$

The activation of PDS with dissolved Fe ions as a catalyst has some intrinsic drawbacks [15]. As shown in **reaction 2**, one mole of added Fe^{2+} only produce one mole of radicals. Although Fe^{2+} can be regenerated via **reactions 4** and **7**, the regeneration rate of Fe^{2+} remains far lower than their consumption rate via **reaction 2** [12, 13]. For efficient production of $SO_4^{\cdot-}$, engineers normally choose to add more Fe^{2+}. The separation of Fe ions as ferric oxyhydroxides is required before discharging treated wastewater into natural waters, resulting in the production of iron sludge. Correspondently, the high cost of the disposal of iron sludge significantly limits the widespread

use of the Fe^{2+}/PDS reaction. Although PDS oxidation processes initiated by heterogeneous catalysts have the potential to avoid iron sludge formation, the application of some of these catalysts leads to problems, such as leaching of metal ions into the acidic solution [16]. Furthermore, other efforts to accelerate the transformation of Fe^{3+} into Fe^{2+} have been undertaken. Hydroxylamine in the Fenton process and the Fe^{2+}/PMS process is reported to enhance the Fe^{3+}/Fe^{2+} redox cycles, which leads to steady Fe^{2+} recovery and significantly activated H_2O_2/PMS with a small addition of Fe ions (1 mg/L) [17, 18]. Hydroxylamine is degraded in oxidation processes, but it also introduces NO_2^-/NO_3^- into the wastewater. Anett *et. al* explored H_2/Pd pairs as a reductant/catalyst to achieve the fast regeneration of Fe^{3+} back to Fe^{2+} and an accelerated catalytic Fenton reaction with traces of iron [9]. It can be concluded from these studies that the continuous regeneration of Fe^{2+} occurs in the presence of a reductive substance.

Based on its excellent performance in the reductive dechlorination of various by-products, electrochemical systems with Pd-modified particle electrodes, namely three-dimensional (3D) electrochemical systems, are also promising systems for the acceleration of Fe^{3+}/Fe^{2+} recycling [21, 22]. Pd catalysts have the unique ability to activate H_2 to form continuously adsorbed atomic H*, which has been confirmed to be a strong reducing agent in catalytic reduction process [23]. Furthermore, compared to an electro-reduction system with a traditional two-dimensional (2D) cathode, a 3D electrochemical system provides a larger surface area and more active sites, significantly improving the electro-reduction capacity [24, 25]. In the work by Qin *et. al*, it was deduced that Fe^{2+} continuously came from the reduction of Fe^{3+} by chemisorbed atomic H* on Au/Pd particle electrodes [26]. However, no direct evidence was provided in their study and, to our knowledge, no study has quantified the accelerating effect of a 3D electrochemical system on Fe^{2+} regeneration and sludge reduction.

In this work, benzoic acid (BA) was used as a probe for $SO_4^{\cdot-}$ and ·OH because BA is highly reactive with these two radicals [27, 28]. First, a trace iron-based electro/Fe^{3+}/PDS system was constructed using Pd/Al_2O_3 as the particle electrode and by externally added PDS as the oxidant. The oxidation performance of this new system was assessed by comparing it with other systems and the radicals in this process were confirmed via electron spin resonance (ESR) analysis and quenching experiments. Thereafter, the influencing factors such as PDS concentration, current density, iron concentration and gas atmosphere were investigated to evaluate the radical utilisation efficiency. Finally, the stability of Pd/Al_2O_3 was studied and the application potential of this system was discussed.

2. Experimental Section

2.1 Chemicals and Materials

Benzoic acid (BA), sodium peroxydisulfate (PDS), ferric sulfate ($Fe_2(SO_4)_3$), sodium sulfate ($NaSO_4$), methanol, tert-butyl alcohol (TBA), and 5,5-dimethyl-1-pyrroline N-oxide (DMPO) were purchased from Sigma Aldrich (Finland).

The Pd/Al_2O_3 catalyst was purchased from Sigma Aldrich (Finland), which had 10% Pd loading on Al_2O_3.

2.2 Experimental Procedures

The solutions in this study were prepared using deionised (DI) water (resistivity of 18.2 MΩ, Arium® Pro System). The solution pH was adjusted using either 100 mM NaOH or 50 mM H_2SO_4. Experiments were conducted in a two-cell electrochemical reactor, a schematic diagram of which is presented in **Figure SM-2** (**Supplementary Material**). Before the reactor was used, N_2 was used to flush out the air in the cathode cell. The hydrogen produced from the cathode was sealed in the cathode cell during the experiment. To prevent further oxidation of BA in the sample, an

ethanol solution was added once the sample was removed from the reactor.

2.3 Analytical Methods

The concentration of BA was measured by high-performance liquid chromatography (HPLC, Shimadzu LC-20AD, Tokyo, Japan) using a C18 column and ultraviolet detector. The mobile phase was maintained at a flow rate of 1.0 mL/min with a constant ratio (50:50) of 25 mM acetic acid and methanol; the temperature of the column was kept at 35 ℃, and the maximum absorption wavelength at 228 nm was selected. The PDS concentration was determined colorimetrically using potassium titanium oxalate solution at a wavelength of 352 nm using an ultraviolet spectrophotometer (Lambda 45, PerkinElmer). This detection method was described in detail by Zeng et al [29]. The Pd leaching concentration was analysed by inductively coupled plasma-optical emission spectroscopy (ICP Agilent 5110).

The formation of reactive oxygen radicals was identified using an electron spin resonance (ESR) spectrometer (CMS 8400, Adani). For the $OH\cdot$ and $SO_4^{\cdot-}$ measurements, the sample was immediately mixed with DMPO to form adducts. The phase composition of the synthesised catalyst was studied using an X-ray diffractometer (XRD, PANalytical) using Co-Kα radiation (λ=0.1789 nm, at 40 kV and 40 mA) over a 2θ range of 10-120° with a step size of 0.02° and scan speed of 2°/min.

3. Results and Discussion

3.1 Enhancement of the Electro/Fe^{2+}/PDS process using Pd/Al_2O_3

Initially, we conducted an experiment to degrade BA (C_0=180 μM) in a Pd/Al_2O_3-enhanced electro/Fe^{3+}/PDS system (Pd-EFP system), *i. e.* in addition to PDS (10 mM) and Fe^{3+} (2 mg or 36 μM), the reaction suspension contained Pd/Al_2O_3 as the particle electrode catalyst and cathode (3.33 mA/cm^2, pH of 3.0, and N_2 atmosphere). As shown in **Figure 1a**, 80.12% of BA was

144 degraded within 120 min. The Pd/Al_2O_3 catalyst in this experiment showed almost no adsorption
145 towards BA or Fe ions.
146 To clarify the role of PDS, the cathode, Pd/Al_2O_3 catalyst, and Fe^{3+} in the oxidation process, control
147 experiments were conducted by excluding each component. Zero degradation of BA occurred in
148 the absence of PDS (electro/Pd/Fe^{3+} system), which obviously played the role of oxidant in the
149 Pd-EFP system. The addition of the Pd/Al_2O_3 catalyst in the Fe^{3+}/PDS system also had a negligible
150 effect on the degradation of BA (Pd/Fe^{3+}/PDS system). To our surprise, 2.87% of BA was degraded
151 in the electro/Fe^{3+}/PDS system. According to the aforementioned discussion, Fe^{3+} could be
152 reduced on the cathode directly and then led to the subsequent activation of PDS [19]. The low
153 reduction efficiency of Fe^{3+} could be ascribed to the occupation of active sites by H^+ and
154 subsequent H_2 evolution on the cathode (**Figure SM-3a**). This was verified by the large amount
155 of bubbles near the cathode. According to the research reported by Anett, generated H_2 can be
156 chemically adsorbed by the Pd/Al_2O_3 catalyst and converted into a strongly reducing agent (Pd-
157 H^*) (**reaction 8**), which can reduce Fe^{3+} [9]. To verify our hypothesis for our system, we
158 investigated the variation of the Fe^{2+} concentration in the Pd-EFP system in the absence of BA and
159 PDS (**Figure 1b**). Because the recycling of Fe^{3+}/Fe^{2+} was too fast to detect the variation of the Fe^{2+}
160 concentration, we increased the initial concentration of Fe ions ten-fold. In the absence of the
161 Pd/Al_2O_3 catalyst, no variation in the iron species was observed. With the addition of 50 mg of
162 Pd/Al_2O_3 in the electrochemical cell, 360 μM of Fe^{3+} could be totally reduced, and Fe^{2+} were
163 formed in only 1 min. The results strongly supported our hypothesis that the cathode played the
164 role of electron donor by electro-generating H_2.

$$\equiv Pd\text{-}H_2 \rightarrow 2 \equiv Pd\text{-}H^* \quad (8)$$

165 In summary, this new system exhibited continuously strong oxidation ability when we applied PDS

as the oxidant, a cathode as an electron donor, Pd/Al_2O_3 particles for the catalytic reduction of Fe^{3+}, and Fe ions as the one-electron transferring medium. Based on this, it is reasonable to divide the Pd-EFP system into a two-stage process: an accelerated Fe^{3+}/Fe^{2+} cycle on the Pd/Al_2O_3 particle electrode and a subsequent Fe^{2+}/PDS oxidation process in the bulk solution.

3.2 Active radical analysis

ESR spectroscopy with the spin-trapping reagent of DMPO was applied to directly confirm the generation of radicals. The hyperfine splitting constants for the DMPO radical adducts of DMPO·-OH and DMPO·-SO_4 were representative of ·OH and $SO_4^{\cdot-}$, respectively [13, 30-32]. In this study, as shown in **Figure 2a**, we observed no signal for the Fe^{3+}/PDS system. For the Pd-EFP system, as we predicted, slight signals for DMPO·-SO_4 adducts suggested the generation of $SO_4^{\cdot-}$. Moreover, a typical four-line ESR spectrum with an intensity of 1:2:2:1 was detected, which indicated the emergence of ·OH.

It is obvious that $SO_4^{\cdot-}$ came from the PDS activation via *in situ*-generated Fe^{2+} (**reaction 2**) in the Pd-EFP system. The redox potential of $SO_4^{\cdot-}$ was confirmed to be 2.5~3.1 V, while the 2.7 V potential of ·OH was detected in acidic solution [33, 34]. Due to the narrow gap of potentials between the two radicals, ·OH could be generated via fast transformation from $SO_4^{\cdot-}$ (**reaction 9**).

$$SO_4^{\cdot-} + H_2O \rightarrow SO_4^{2-} + \cdot OH + H^+ \quad (9)\ [12]$$

Quenching experiments were further conducted to check the importance of $SO_4^{\cdot-}$ and ·OH in the oxidation process. Ethanol is well known to be an efficient scavenger for ·OH and $SO_4^{\cdot-}$ due to its high reaction constant with these two radicals [34]. As shown in **Figure 2b**, the degradation of BA was significantly inhibited in the presence of ethanol. More specifically, 80.12% BA was degraded without ethanol within 120 min. With the addition of 0.18 M ethanol, only 30.80% BA degradation

was observed; with a further increase in the ethanol concentration to 1.8 M, the degradation of BA was reduced to 22.82%. The inhibitory effect of ethanol on the BA degradation indicated that $SO_4^{\cdot-}$ and its symbiotic radical (·OH) were the main oxidation species in the Pd-EFP system.

The reductive effect of Pd-based catalysts in the electrochemistry system has been extensively investigated [21, 22, 35, 36]. Direct electron transfer and atomic H* may be both involved in the accelerated recycling process of Fe^{3+}/Fe^{2+}. For a better understanding of the accelerated iron recycling process, we further clarified the importance of the two reductive mechanisms in the reduction process of Fe^{3+}. Tert-butyl alcohol (TBA) is reported to be an efficient scavenging agent of atomic H* [21]. To minimise the systematic error, the initial Fe^{3+} concentration was increased to 360 μM, while the Pd/Al_2O_3 catalyst was set to only 5.0 mg/120 mL. As shown in **Figure 3**, strong inhibition of Fe^{3+} reduction occurred with TBA addition (36 mM and 360 mM). We further fitted the process with pseudo-first-order kinetics. As shown in **Figure 3** (insert), with TBA additions of 36 mM and 360 mM, the reduction kinetics constant decreased by 77.81% and 83.97%, respectively. The sharp decrease in the Fe^{3+} reduction rate suggested the main role of atomic H* rather than direct electron transfer on the Pd/Al_2O_3 particle electrode (**reaction 10, Figure SM-3b**), which is identical to the catalytic property of Pd as an atomic H* keeper.

$$\equiv Pd\text{-}H^* + Fe^{3+} \rightarrow \equiv Pd + H^+ + Fe^{2+} \quad (10)$$

TBA is also an effective screening agent for ·OH because it exhibits a low reactivity towards $SO_4^{\cdot-}$ [34]. Consequently, the inhibitory effect of TBA on organic degradation is normally not stronger than that of ethanol for normal oxidation processes. Interestingly, the screening effect of TBA on BA degradation in our system was stronger than the influence of ethanol (**Figure 2b**) [18]. This contradiction can be ascribed to the simultaneous inhibition of both ·OH and atomic H*. The results further confirmed the importance of atomic H* for the reduction of Fe^{3+}.

Atomic H* may originate from the adsorption of electrogenerated H_2 or H^+ conversion via electro-induction on the Pd surface [9]. Plenty of atomic H* in the bulk solution accelerated the transformation of Fe^{3+} to Fe^{2+} considerably. The Pd-EFP system provided continuous Fe^{2+} for the Fe^{2+}/PDS oxidation process. Thus, organics could be degraded by both $SO_4^{\cdot-}$ and ·OH from the Fe^{2+}-activated PDS process.

3.3 Sludge production

Fe ions bridged as a single electron-transferring medium between the electron-donor and PDS-oxidation process. Additionally, Fe ions are significant for this system because they are removed from water as a sludge, which is the focus of our research. We then investigated the effect of varying the initial iron concentration on the efficiency of BA. As shown in **Figure 4**, with the addition of 180 μM Fe^{3+} (10 mg/L), the degradation efficiency of BA was determined to be 86.89% within 120 min. When we further decreased the initial Fe^{3+} concentration to 36 μM (2 mg/L), the removal efficiency was kept at 80.12%.

To quantitatively compare the iron sludge production in various systems, we standardized the iron sludge production by dividing the iron dosage (C_0(Fe)) by the organic removal (ΔC(pollutant)) in the Fe^{2+}/PDS process. Depending on the organic contaminants, the ratio varied from 5.1 to 238 for the Fe^{2+}/PDS process (**Table 1**) [37-43]. As shown in **reactions 2-7**, one mole of Fe^{2+} can produce one mole of ·OH, which can subsequently oxidize up to one mole of organics. Thus, a ratio of C(Fe)/ΔC(pollutant) in the Fe^{2+}-activated PDS process below 1.0 indicates the recycling of Fe ions in the system. We checked the C(Fe)/ΔC(BA) in the Fe^{2+}/PDS oxidation process of BA (**Table 1**), and the ratio was 87.2 when the ratio was decreased to 0.2 in the Pd-EFP system, suggesting trace production of iron sludge in the post-treatment process.

For conventional Fenton processes or Fe^{2+}/PDS processes, excess Fe^{2+} has been reported to have

a detrimental effect on the oxidation of contaminants owing to their quenching effect toward ·OH and $SO_4^{\cdot-}$ (**reactions 11-12**). According to studies on Fe^{2+}/PDS processes (**Table 1**), an optimal ratio of C(Fe)/C(PDS) for organic degradation has generally been determined to be in the range of 0.16-1.0 [37-43]. With higher Fe^{2+} addition than the optimal dosage, excess Fe^{2+} will result in decreasing the degradation efficiency of organics. We checked the BA degradation in the Fe^{2+}/PDS system, and the optimal ratio was obtained when the iron concentration was 1.5 times the PDS concentration (**Figure SM-4**). In the Pd-EFP process, the Fe^{2+}/PDS ratio was no more than 0.0036, indicating that Fe^{2+} was mainly used for PDS activation instead of radical quenching. The addition of trace iron not only benefited the post treatment of the dissolved iron, but also improved the contaminant oxidation efficiency of the Fe^{2+}/PDS process.

$$Fe^{2+} + \cdot OH \rightarrow Fe^{3+} + OH^- \quad (11)\ [9]$$

$$Fe^{2+} + SO_4^{\cdot-} \rightarrow Fe^{3+} + SO_4^{2-} \quad (12)\ [7]$$

Another mechanism for decreasing the iron dosage in the Fe^{2+}-activating oxidation process is the reduction of Fe^{3+} on the cathode (**reaction 13**), which has been widely investigated for the electro-Fenton process. By accurately controlling the applied potential on the cathode, such as graphite or carbon felt, fast reduction of Fe^{3+} can be achieved.

$$Fe^{3+} + e^- \rightarrow Fe^{2+} \quad (13)$$

To better compare the performance of this new system and electro-Fenton system on the iron sludge reduction, the iron concentration in electro-Fenton processes are summarised in **Table SM-1**. Obviously, the electro-Fenton process requires iron dosages according to the different cathode materials. To continuously provide Fe^{2+} and activate H_2O_2, iron concentrations are required to be higher than 0.2 mM (11.2 mg/L). In contrast, the iron dosage was 36 μM (2 mg/L) in the Pd-EFP system (limitation of Fe in EU and US). The further decrease in the need for iron can be ascribed

to the strong reduction ability of atomic H* and large surface area of the Pd/Al_2O_3 catalyst.

3.4 Radical consumption analysis

The effects of the applied current density and PDS concentration were investigated to optimize the parameters and explore side reactions. As shown in **Figure 5a**, under a current density of 0.66 mA/cm^2, the degradation efficiency of BA was only 20.63% within 120 min. With an increase in the current density to 3.33 mA/cm^2, the degradation efficiency was improved to 80.12%. Interestingly, a further increase in the current density to 6.66 mA/cm^2 led to a counterproductive effect on BA degradation.

With the increase in the current density, the applied voltage increased and hydrogen bubbles were produced faster, both of which were beneficial to the production of atomic H* on the Pd/Al_2O_3. Thus, as a reductant, atomic H* on the catalyst can act not only as an accelerator of iron recycling but also as a possible quenching agent for ·OH and $SO_4^{\cdot-}$ (**reactions 14-15**). The adverse effect of current density beyond 3.33 mA/cm^2 verified the hypothesis, *i. e.* in our system, the optimal current density was 3.33 mA/cm^2.

$$\equiv Pd\text{-}H^* + \cdot OH \rightarrow \equiv Pd + H^+ + OH^- \quad (14)$$

$$\equiv Pd\text{-}H^* + SO_4^{\cdot-} \rightarrow \equiv Pd + H^+ + SO_4^{2-} \quad (15)$$

Similar to the effect of current density on the performance of BA degradation, BA removal was enhanced with an increase in the PDS concentration from 2 to 20 mM; however, a further increase of PDS concentration adversely affected the degradation efficiency of BA (**Figure 5b**). This was due to the fact that more $SO_4^{\cdot-}$ was generated at higher PDS concentrations, but excessive PDS consumed $SO_4^{\cdot-}$ via **reaction 3** [44].

3.5 Effect of the gas atmosphere

The gas atmosphere above the cathodic cell is another parameter that affects the reaction on the

273 Pd/Al_2O_3. We concluded that atomic H* is the main species responsible for Fe^{3+} reduction. It has
274 been found that dissolved oxygen can compete with Fe^{3+} for the reaction with atomic H* (**reaction**
275 **16**) [45, 46]. Given the inhibition of dissolved oxygen on atomic H*, oxygen should be prevented
276 in the cathodic cell.

$$4 \equiv Pd\text{-}H^* + O_2 \rightarrow 4 \equiv Pd + 2\ H_2O \quad (16)\ [47]$$

277 In the study by Anett *et.al*, increasing concentration of H_2 above the cathode cell was found to be
278 beneficial to accelerate Fe^{3+} recycling owing to the reductive effect of activated H_2 on the Pd/Al_2O_3
279 catalyst [9]. By slowly feeding N_2 and H_2, we checked the performance of the Pd-EFP process on
280 BA degradation in N_2 and H_2 atmospheres (**Figure 6a**). Compared with the *in situ* electro-
281 generated H_2 atmosphere, pure N_2 provided a better atmosphere for the performance of the Pd-
282 EFP system on BA degradation. Interestingly, PDS in the H_2 atmosphere initially displayed a
283 higher degradation rate than in the N_2 atmosphere, but almost no degradation of BA occurred after
284 a retention time of 40 min. This variation can be ascribed to the quick degradation of PDS in the
285 pure H_2 atmosphere. As shown in **Figure 6b**, the PDS was degraded quickly in the pure H_2
286 atmosphere, while N_2 and electro-generated H_2 atmospheres showed a relatively slow degradation
287 rate towards PDS. The results indicated a two-electron transfer from H_2 to PDS via **reaction 17**
288 rather than one-electron transfer from atomic H* to Fe^{3+}, which suppresses the oxidation process
289 via a $Pd\text{-}H^* \rightarrow Fe^{3+}/Fe^{2+} \rightarrow PDS/SO_4^{\cdot -} \rightarrow$BA mechanism. To confirm this hypothesis, we checked
290 BA degradation in the H_2/Pd/PDS system, and PDS was completely consumed with zero
291 degradation of BA.

$$\equiv Pd\text{-}H_2 + S_2O_8^{2-} \rightarrow \equiv Pd + 2\ H^+ + 2\ SO_4^{2-} \quad (17)$$

292 By dispelling accumulated H_2 above the reaction liquid and suppressing the oxygen reduction, N_2
293 atmosphere could steer the reaction on the surface of Pd/Al_2O_3 in the right direction toward Fe^{3+}

reduction by atomic H*, further leading to efficient organic degradation.

3.6 Application potential analysis

The aforementioned results indicated that Pd/Al_2O_3 particles, as a famous H^* keeper, showed high performance for iron recycling and reduction of iron sludge production in the Fe^{2+}/PDS process. According to our catalyst dosage study, even with the addition of only 10 mg Pd/Al_2O_3 catalyst per 120 mL of reaction liquid in the Pd-EFP system, BA degradation could reach the level of 60% (**Figure SM-5**). However, the stability of the particle electrode is a crucial issue owing to the high cost of noble metals. The Pd/Al_2O_3 catalyst has been extensively used in chemical industries owing to its high stability and outstanding catalytic efficiency [23]. We also monitored the catalyst stability by recycling the Pd/Al_2O_3 catalyst in the Pd-EFP system five times. As shown in **Figure 7a**, the degradation efficiencies were kept relatively stable between 80.56% and 83.19%, indicating relatively high stability. Simultaneously, the Pd concentration in the effluent was lower than the detection limit of ICP-OES (0.01 mg/L). The variation in the catalytic activity on the Pd/Al_2O_3 catalyst in the Pd-EFP process was evaluated using XRD analysis. XRD patterns of the fresh and used Pd/Al_2O_3 catalyst were recorded, as shown in **Figure 7b**, where diffraction peaks assigned to (111), (200), and (311) of metallic Pd were observed. The obtained results demonstrated that Pd/Al_2O_3 is stable and could be effectively used for a long period of time, which can produce a considerable economic benefit.

For practical application, the initial solution pH and the variation of the solution pH with the reaction progress are also important [48, 49]. Owing to the acidification effect of the PDS decomposition process (**reaction 17**), the Pd-EFP process was confirmed to be an efficient system even with an initial solution pH of 10.0. (**Text SM-2**).

The Pd-EFP process successfully produced a continuous Fe^{2+}/PDS process with trace amounts of

317 Fe ions. However, this also resulted in some drawbacks, such as a low oxidation rate, high cost for
318 catalyst preparation, and subsequent recovery of the Pd/Al_2O_3 catalyst. The catalyst dosage
319 analysis revealed that the Pd-EFP process exhibited oxidation capacity even when we used a Pd
320 catalyst dosage of 10 mg/120 mL (**Figure SM-5**). Furthermore, in the research field of
321 electrocatalytic dechlorination, various functional materials have been developed that possess new
322 characteristics while maintaining their capacity as an atomic H* keeper, and they are good
323 alternatives as particle electrodes in this system. To further decrease the Pd dosage in the Pd-EFP
324 system, the catalytic activity of atomic H* formation can be enhanced by changing the morphology
325 so that the Pd(111) facet and defect sites on the Pd crystal are highly active [50, 51]. It has been
326 found that Pd-supported multi-walled nanotubes can act as an excellent H* producer in a 3D
327 electrocatalytic process with only 0.5% loading of Pd [22]. A bimetal catalyst (Pd/In) has also
328 showed strong reductive capacity in a 3D electrochemical process [21]. This research points out
329 the novel approach of reducing the iron sludge in the Fe^{2+}-activated peroxide process by
330 accelerating the transformation from Fe^{3+} to Fe^{2+} using surface-bound atomic H* on Pd/Al_2O_3.
331 Other atomic H* keeper materials should be tested to evaluate the application value of this
332 technology in the future.

333 **4. Conclusion**

334 In this study, a trace-iron based electro/Fe^{3+}/PDS system was constructed using Pd/Al_2O_3 as the
335 particle electrode and by externally added PDS as the oxidant. At an initial solution pH of 3.0, with
336 the addition of 10 mM PDS, 50 mg Pd/Al_2O_3, and 2 mg/L Fe ions, 80.12% of 180 μM BA was
337 degraded within 120 min. Mechanistic studies showed that the ·OH and $SO_4^{\cdot-}$ from Fe^{2+}-activated
338 PDS were responsible for the BA degradation, whereas atomic H* was mainly responsible for Fe^{3+}
339 reduction to Fe^{2+}. In the Pd-EFP process, the optimal dosage of Fe ions was determined to be 36

μM (2 mg/L) because the extra addition of more than 2 mg/L Fe ions had a positive but negligible influence on BA degradation. Correspondently, the optimal current density and PDS concentration in the Pd-EFP system were found to be 3.33 mA/cm^2 and 20 mM, respectively. A higher current density or higher PDS concentration had a quenching effect on $SO_4^{\cdot-}$. The Pd-EFP process is efficient for BA degradation at various initial solution pH levels. Furthermore, the degradation of BA was also efficiently promoted by the N_2 atmosphere, which could steer the reaction on the surface of Pd/Al_2O_3 in the right direction toward Fe^{3+} reduction by atomic H* by dispelling accumulated H_2 above the reaction liquid and suppressing oxygen reduction. Finally, catalyst reusability experiments and the XRD pattern of fresh and used Pd/Al_2O_3 catalyst indicated that the Pd/Al_2O_3 catalyst maintained its high durability in the Pd-EFP system.

Supporting information

Two texts, 5 figures and 1 table are available in the Supplementary Material.

Acknowledgements

The authors are grateful to the Academy of Finland and the European Union for funding this project.

References

[1] B.C. Hodges, E.L. Cates, J.H. Kim, Challenges and prospects of advanced oxidation water treatment processes using catalytic nanomaterials, Nat. Nanotechnol. 13 (2018) 642-650. https://doi.org/10.1038/s41565-018-0216-x.

[2] L. Li, C. Lai, F. Huang, M. Cheng, G. Zeng, D. Huang, B. Li, S. Liu, M. Zhang, L. Qin, M. Li, J. He, Y. Zhang, L. Chen, Degradation of naphthalene with magnetic bio-char activate hydrogen peroxide: Synergism of bio-char and Fe-Mn binary oxides, Water Res. 160 (2019) 238-248. https://doi.org/10.1016/j.watres.2019.05.081.

[3] C. Zhou, P. Xu, C. Lai, C. Zhang, G. Zeng, D. Huang, M. Cheng, L. Hu, W. Xiong, X. Wen, L. Qin, J. Yuan, W. Wang, Rational design of graphic carbon nitride copolymers by molecular doping for visible-light-driven degradation of aqueous sulfamethazine and hydrogen evolution, Chem. Eng. J. 359 (2019) 186-196. https://doi.org/10.1016/j.cej.2018.11.140.

[4] C. Zhou, D. Huang, P. Xu, G. Zeng, J. Huang, T. Shi, C. Lai, C. Zhang, M. Cheng, Y. Lu, A. Duan, W. Xiong, M. Zhou, Efficient visible light driven degradation of sulfamethazine and tetracycline by salicylic acid modified polymeric carbon nitride via charge transfer, Chem. Eng. J. 370 (2019) 1077-1086. https://doi.org/10.1016/j.cej.2019.03.279

[5] J.J. Pignatello, E. Oliveros, A. MacKay, Advanced oxidation processes for organic contaminant destruction based on the Fenton reaction and related chemistry, Crit. Rev. Environ. Sci. Technol. 36 (2006) 1-84. https://doi.org/10.1080/10643380500326564.

[6] T. Olmez-Hanci, I. Arslan-Alaton, Comparison of sulfate and hydroxyl radical based advanced oxidation of phenol, Chem. Eng. J. 224 (2013) 10-16. https://doi.org/10.1016/j.cej.2012.11.007

[7] I.M. Kolthoff, A.I. Medalia, H.P. Raaen, The reaction between ferrous iron and peroxides. IV. Reaction with potassium persulfate[1a], J. Am. Chem. Soc. 73 (1951) 1733-1739. https://doi.org/10.1021/ja01148a089.

[8] H. Kusic, I. Peternel, S. Ukic, N. Koprivanac, T. Bolanca, S. Papic, A.L. Bozic, Modeling of iron activated persulfate oxidation treating reactive azo dye in water matrix, Chem. Eng. J. 172 (2011) 109-121. https://doi.org/10.1016/j.cej.2011.05.076.

[9] A. Georgi, M.V. Polo, K. Crincoli, K. Mackenzie, F.D. Kopinke, Accelerated catalytic Fenton reaction with traces of iron: An Fe-Pd-multicatalysis approach, Environ. Sci. Technol. 50 (2016) 5882-5891. https://doi.org/10.1021/acs.est.6b01049.

[10] R. Woods, I. Kolthoff, E.J. Meehan, Arsenic(IV) as an intermediate in the induced oxidation of arsenic(III) by the iron(II)-persulfate reaction. J. Am. Chem. Soc. 86 (1964) 1698-1700. https://doi.org/10.1021/ja01063a011.

[11] H.Z. Liu, T.A. Bruton, F.M. Doyle, D.L. Sedlak, In situ chemical oxidation of contaminated groundwater by persulfate: Decomposition by Fe(III)- and Mn(IV)-containing oxides and aquifer materials, Environ. Sci. Technol. 48 (2014) 10330-10336. https://doi.org/10.1021/es502056d.

[12] C.J. Liang, H.W. Su, Identification of sulfate and hydroxyl radicals in thermally activated persulfate, Ind. Eng. Chem. Res. 48 (2009) 5558-5562. https://doi.org/10.1021/ie9002848.

[13] O.S. Furman, A.L. Teel, R.J. Watts, Mechanism of base activation of persulfate, Environ. Sci. Technol. 44 (2010) 6423-6428. https://doi.org/10.1021/es1013714.

[14] W.P. Kwan, B.M. Voelker, Decomposition of hydrogen peroxide and organic compounds in the presence of dissolved iron and ferrihydrite, Environ. Sci. Technol. 36 (2002) 1467-1476. https://doi.org/10.1021/es011109p.

[15] A. Rastogi, S.R. Al-Abed, D.D. Dionysiou, Effect of inorganic, synthetic and naturally occurring chelating agents on Fe(II) mediated advanced oxidation of chlorophenols, Water Res. 43 (2009) 684-694. https://doi.org/10.1016/j.watres.2008.10.045.

[16] M. Hartmann, S. Kullmann, H. Keller, Wastewater treatment with heterogeneous Fenton-type catalysts based on porous materials, J. Mater. Chem. 20 (2010) 9002-9017. https://doi.org/10.1039/C0JM00577K.

[17] L.W. Chen, J. Ma, X.C. Li, J. Zhang, J.Y. Fang, Y.H. Guan, P.C. Xie, Strong enhancement on Fenton oxidation by addition of hydroxylamine to accelerate the ferric and ferrous iron cycles, Environ. Sci. Technol. 45 (2011) 3925-3930. https://doi.org/10.1021/es2002748.

[18] J. Zou, J. Ma, L.W. Chen, X.C. Li, Y.H. Guan, P.C. Xie, C. Pan, Rapid acceleration of ferrous iron/peroxymonosulfate oxidation of organic pollutants by promoting Fe(III)/Fe(II) cycle with hydroxylamine, Environ. Sci. Technol. 47 (2013) 11685-11691. https://doi.org/10.1021/es4019145.

[19] Y.Y. Chu, Y. Qian, W.J. Wang, X.L. Deng, A dual-cathode electro-Fenton oxidation coupled with anodic oxidation system used for 4-nitrophenol degradation, J. Hazard. Mater. 199 (2012) 179-185. https://doi.org/10.1016/j.jhazmat.2011.10.079.

[20] C. Ridruejo, F. Centellas, P.L. Cabot, I. Sires, E. Brillas, Electrochemical Fenton-based treatment of tetracaine in synthetic and urban wastewater using active and non-active anodes, Water Res. 128 (2018) 71-81. https://doi.org/10.1016/j.watres.2017.10.048

[21] H.C. Lan, R. Mao, Y.T. Tong, Y.Z. Liu, H.J. Liu, X.Q. An, R.P. Liu, Enhanced electroreductive removal of bromate by a supported Pd-In bimetallic catalyst: kinetics and mechanism investigation, Environ. Sci. Technol. 50 (2016) 11872-11878. https://doi.org/10.1021/acs.est.6b02822.

[22] X.Y. She, Q. Yang, F.B. Yao, Y. Zhong, W.C. Ren, F. Chen, J. Sue, Y.H. Ma, Z.Y. Fe, D.B. Wang, X.M. Li, Electrocatalytic hydrodechlorination of 4-chlorophenol on Pd supported multi-walled carbon nanotubes particle electrodes, Chem. Eng. J. 358 (2019) 903-911. https://doi.org/10.1016/j.cej.2018.10.095.

[23] B.P. Chaplin, M. Reinhard, W.F. Schneider, C. Schuth, J.R. Shapley, T.J. Strathmann, C.J. Werth, Critical review of Pd-based catalytic treatment of priority contaminants in water, Environ. Sci. Technol. 46 (2012) 3655-3670. https://doi.org/10.1021/es204087q.

[24] R. Mao, X. Zhao, H.C. Lan, H.J. Liu, J.H. Qu, Graphene-modified Pd/C cathode and Pd/GAC particles for enhanced electrocatalytic removal of bromate in a continuous three-dimensional electrochemical reactor, Water Res. 77 (2015) 1-12. https://doi.org/10.1016/j.watres.2015.03.002.

[25] J. Li, J. Yan, G. Yao, Y. Zhang, X. Li, B.J.C.E.J. Lai, Improving the degradation of atrazine in the three-dimensional (3D) electrochemical process using $CuFe_2O_4$ as both particle electrode and catalyst for persulfate activation, Chem. Eng. J. 361 (2018) 1317-1332. https://doi.org/10.1016/j.cej.2018.12.144.

[26] Y.H. Qin, M. Sun, H.J. Liu, J.H. Qu, AuPd/Fe_3O_4-based three-dimensional electrochemical system for efficiently catalytic degradation of 1-butyl-3-methylimidazolium hexafluorophosphate, Electrochim. Acta. 186 (2015) 328-336. https://doi.org/10.1016/j.electacta.2015.10.122.

[27] M.E. Lindsey, M.A. Tarr, Quantitation of hydroxyl radical during Fenton oxidation following a single addition of iron and peroxide, Chemosphere 41 (2000) 409-417. https://doi.org/10.1016/S0045-6535(99)00296-9.

[28] P. Nate, V. Madhavan, H. Zemel, R.J.J.A.C.S. Fessenden, Rate constants and mechanism of reaction of $SO_4^{\cdot-}$ with aromatic compounds, J. Am. Chem. Soc. 99 (1977) 163-164. http://doi.org/10.1021/ja00443a030.

[29] H.B. Zeng, S.S. Liu, B.Y. Chai, D. Cao, Y. Wang, X. Zhao, Enhanced photoelectrocatalytic decomplexation of Cu-EDTA and Cu recovery by persulfate activated by UV and cathodic reduction, Environ. Sci. Technol. 50 (2016) 6459-6466. https://doi.org/10.1021/acs.est.6b00632.

[30] P.L. Zamora, F.A. Villamena, Theoretical and experimental studies of the spin trapping of inorganic radicals by 5,5-dimethyl-1-pyrroline N-oxide (DMPO). 3. sulfur Dioxide, sulfite, and sulfate radical anions, J. Phys. Chem. A. 116 (2012) 7210-7218. https://doi.org/10.1021/jp3039169.

[31] C. Zhou, C. Lai, P. Xu, G. Zeng, D. Huang, C. Zhang, M. Cheng, L. Hu, J. Wan, Y. Liu, W. Xiong, Y. Deng, M. Wen, In Situ Grown AgI/$Bi_{12}O_{17}C_{l2}$ Heterojunction Photocatalysts for Visible Light Degradation of Sulfamethazine: Efficiency, Pathway, and Mechanism, ACS Sustain. Chem. Eng. 6 (2018) 4174-4184. https://doi.org/10.1021/acssuschemeng.7b04584.

[32] C. Zhou, C. Lai, P. Xu, G. Zeng, D. Huang, Z. Li, C. Zhang, M. Cheng, L. Hu, J. Wan, F. Chen, W. Xiong, R. Deng, Rational Design of Carbon-Doped Carbon Nitride/$Bi_{12}O_{17}C_{l2}$ Composites: A Promising Candidate Photocatalyst for Boosting Visible-Light-Driven Photocatalytic Degradation of Tetracycline, ACS Sustain. Chem. Eng. 6 (2018) 6941-6949. https://doi.org/10.1021/acssuschemeng.8b00782.

[33] G.V. Buxton, C.L. Greenstock, W.P. Helman, A.B. Ross, Critical review of rate constants for reactions of hydrated electrons, hydrogen atoms and hydroxyl radicals (·OH/$\cdot O^-$) in Aqueous Solution, J. Phys. Chem. Ref. Data. 17 (1988) 513-886. https://doi.org/10.1063/1.555805.

[34] P. Neta, R.E. Huie, A.B. Ross, Rate constants for reactions of inorganic radicals in aqueous-solution, J. Phys. Chem. Ref. Data. 17 (1988) 1027-1284. https://doi.org/10.1063/1.555808.

[35] X. Zhao, A. Li, R. Mao, H. Liu, J. Qu, Electrochemical removal of haloacetic acids in a three-dimensional electrochemical reactor with Pd-GAC particles as fixed filler and Pd-modified carbon paper as cathode, Water Res. 51 (2014) 134-143. https://doi.org/10.1016/j.watres.2013.12.028.

471 [36] J. Zhou, Z. Lou, J. Xu, X. Zhou, K. Yang, X. Gao, Y. Zhang, X. Xu, Enhanced electrocatalytic
472 dechlorination by dispersed and moveable activated carbon supported palladium catalyst, Chem.
473 Eng. J. 358 (2019) 1176-1185. https://doi.org/10.1016/j.cej.2018.10.098.
474 [37] X.X. Jiang, Y.L. Wu, P. Wang, H.J. Li, W.B. Dong, Degradation of bisphenol A in aqueous
475 solution by persulfate activated with ferrous ion, Environ. Sci. Pollut. Res. 20 (2013) 4947-4953.
476 https://doi.org/10.1007/s11356-013-1468-5.
477 [38] L. Bu, Z. Shi, S. Zhou, Modeling of Fe(II)-activated persulfate oxidation using atrazine as a
478 target contaminant, Sep. Purif. Technol. 169 (2016) 59-65.
479 https://doi.org/10.1016/j.seppur.2016.05.037.
480 [39] W. Shang, Z. Dong, M. Li, X. Song, M. Zhang, C. Jiang, F. Sun, Degradation of diatrizoate
481 in water by Fe(II)-activated persulfate oxidation, Chem. Eng. J. 361 (2019) 1333-1344.
482 https://doi.org/10.1016/j.cej.2018.12.139.
483 [40] A. Long, Y. Lei, H. Zhang, Degradation of toluene by a selective ferrous ion activated
484 persulfate oxidation process, Industrial & Engineering Chemistry Research 53 (2014) 1033-1039.
485 https://doi.org/10.1021/ie402633n.
486 [41] Y.F. Rao, L. Qu, H. Yang, W. Chu, Degradation of carbamazepine by Fe(II)-activated
487 persulfate process, J. Hazard. Mater. 268 (2014) 23-32.
488 https://doi.org/10.1016/j.jhazmat.2014.01.010.
489 [42] S. Wang, J. Wang, Comparative study on sulfamethoxazole degradation by Fenton and Fe(II)-
490 activated persulfate process, RSC Adv. 7 (2017) 48670-48677.
491 https://doi.org/10.1039/C7RA09325J

[43] L. Zhou, W. Zheng, Y. Ji, J. Zhang, C. Zeng, Y. Zhang, Q. Wang, X. Yang, Ferrous-activated persulfate oxidation of arsenic(III) and diuron in aquatic system, J. Hazard. Mater. 263 (2013) 422-430. https://doi.org/10.1016/j.jhazmat.2013.09.056

[44] W.J. McElroy, S.J. Waygood, Kinetics of the reactions of the $SO_4^{\cdot-}$ radical with $SO_4^{\cdot-}$, $S_2O_8^{2-}$, H_2O and Fe^{2+}, J. Chem. Soc. Faraday Trans. 86 (1990) 2557-2564. https://doi.org/10.1002/chin.199044022.

[45] W. Xie, S. Yuan, X. Mao, W. Hu, P. Liao, M. Tong, A.N. Alshaulabkeh, Electrocatalytic activity of Pd-loaded Ti/TiO_2 nanotubes cathode for TCE reduction in groundwater, Water Res. 47 (2013) 3573-3582. https://doi.org/10.1016/j.watres.2013.04.004.

[46] R. Mao, N. Li, H.C. Lan, X. Zhao, H.J. Liu, J.H. Qu, M. Sun, Dechlorination of trichloroacetic acid using a noble metal-free graphene-Cu foam electrode via direct cathodic reduction and atomic H*, Environ. Sci. Technol. 50 (2016) 3829-3837. https://doi.org/10.1021/acs.est.5b05006.

[47] S. Yuan, Y. Fan, Y. Zhang, M. Tong, P. Liao, Pd-Catalytic In situ generation of H_2O_2 from H_2 and O_2 produced by water electrolysis for the efficient electro-Fenton degradation of rhodamine B, Environ. Sci. Technol. 45 (2011) 8514-8520. https://doi.org/10.1021/es2022939.

[48] Q. Ouyang, F. Kou, N. Zhang, J. Lian, G. Tu, Z. Fang, Tea polyphenols promote Fenton-like reaction: pH self-driving chelation and reduction mechanism, Chem. Eng. J. 366 (2019) 514-522. https://doi.org/10.1016/j.cej.2019.02.078.

[49] L. Hu, G. Zhang, M. Liu, Q. Wang, S. Dong, P. Wang, Application of nickel foam-supported Co_3O_4-Bi_2O_3 as a heterogeneous catalyst for BPA removal by peroxymonosulfate activation, Sci. Total Environ. 647 (2019) 352-361. https://doi.org/10.1016/j.scitotenv.2018.08.003.

[50] R. Liu, H. Zhao, X. Zhao, Z. He, Y. Lai, W. Shan, D. Bekana, G. Li, J. Liu, Defect sites in ultrathin Pd nanowires facilitate the highly efficient electrochemical hydrodechlorination of

pollutants by H*(ads), Environ. Sci. Technol. 52 (2018) 9992-10002. https://doi.org/10.1021/acs.est.8b02740.

[51] P. Quaino, E. Santos, Hydrogen evolution reaction on palladium multilayers deposited on Au(111): A theoretical approach, Langmuir 31 (2015) 858-867. https://doi.org/10.1021/la503881y.

Tables and Figures

Table. 1 A comparison of pollutant concentration, iron dosage and PDS dosage in the Fe^{2+}/PDS system

Figure 1. (a) Degradation efficiency of BA in various systems ([BA], 180 μM; [PDS], 10 mM; [Fe^{3+}], 36 μM; [Pd/Al_2O_3], 50 mg/120 mL; current density, 3.33 mA/cm^2; initial solution pH, 3.0); (b) Reduction ratio of Fe^{3+} in the Pd-EFP system (initial solution pH, 3.0; C(Fe ions), 360 μM)

Figure 2. (a) ESR spectra of DMPO·-OH and DMPO·-SO_4 formed in various systems. (b) Effect of scavengers on the BA degradation in the Pd-EFP system ([BA], 180 μM; [PDS], 10 mM; [Fe^{3+}], 36 μM; [Pd/Al_2O_3], 50 mg/120 mL; current density, 3.33 mA/cm^2; initial solution pH, 3.0)

Figure 3. Fe^{2+} concentration variation in the Pd-EFP system without PDS and BA ([Fe^{3+}], 360 μM; [Pd/Al_2O_3], 50 mg/120 mL; current density, 3.33 mA/cm^2; initial solution pH, 3.0)

Figure 4. Effect of initial Fe^{3+} addition on the removal efficiency of BA in the Pd-EFP system ([BA], 180 μM; [PDS], 10 mM; [Pd/Al_2O_3], 50 mg/120 mL; current density, 3.33 mA/cm^2; initial solution pH, 3.0)

Figure 5. Effect of current density (a) and initial PDS addition (b) on the removal efficiency of BA in the Pd-EFP system ([BA], 180 μM; [PDS], 10 mM; [Fe^{3+}], 36 μM; [Pd/Al_2O_3], 50 mg/120 mL; current density, 3.33 mA/cm^2; initial solution pH, 3.0)

Figure 6. Effect of gas atmosphere in a cathode cell on BA degradation (a) and PDS consumption (b) in the Pd-EFP system ([BA], 180 μM; [PDS], 10 mM; [Fe^{3+}], 36 μM; [Pd/Al_2O_3], 50 mg/120 mL; current density, 3.33 mA/cm^2; initial solution pH, 3.0)

Figure. 7. (a) The degradation efficiency of BA in the Pd-EFP system for five recycling times ([BA], 180 μM; [PDS], 10 mM; [Fe^{3+}], 36 μM; current density, 3.33 mA/cm^2; initial solution pH, 3.0, reaction time, 120 min) (b) XRD spectra of the fresh and used Pd/Al_2O_3 catalysts

Table. 1 A comparison of pollutant concentration, iron dosage and PDS dosage in the Fe^{2+}/PDS system

ΔC(pollutant)	C(Fe)	C(PDS)	C(Fe)/ΔC(pollutant)	C(Fe)/C(PDS)	
40 μM	1.6 mM	2 mM	40	0.16	[37]
10 μM	0.4 mM	0.4 mM	40	1	[38]
4.2 μM	1 mM	5 mM	238	0.2	[39]
0.7 mM	3.6 mM	5 mM	5.1	0.72	[40]
0.84 mM	5.8 mM	20 mM	6.9	0.29	[40]
0.8 mM	8.1 mM	35 mM	10.13	0.23	[40]
25 μM	0.25 mM	1 mM	10	0.25	[41]
50 μM	4 mM	4 mM	80	1	[42]
32 μM	2 mM	2 mM	62.5	1	[43]
172 μM	15 mM	10 mM	87.2	1.5	Fe^{2+}/PDS
144 μM	36 μM	10 mM	0.25	0.0036	Pd-EFP

547

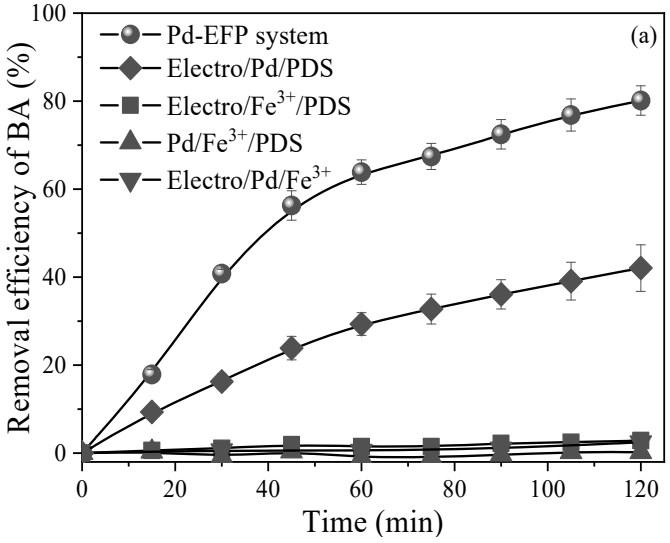

548

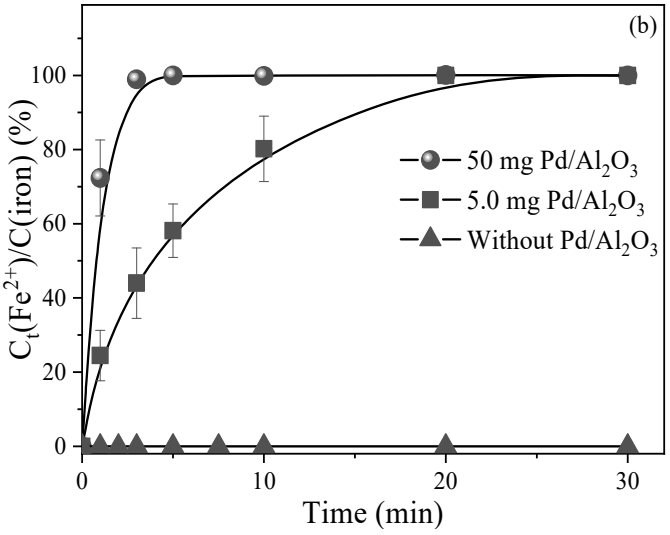

549

550 **Figure 1.** (a) Degradation efficiency of BA in various systems ([BA], 180 μM; [PDS], 10 mM;

551 [Fe^{3+}], 36 μM; [Pd/Al_2O_3], 50 mg/120 mL; current density, 3.33 mA/cm^2; initial solution pH, 3.0);

552 (b) Reduction ratio of Fe^{3+} in the Pd-EFP system (initial solution pH, 3.0; C(Fe ions), 360 μM)

553

554

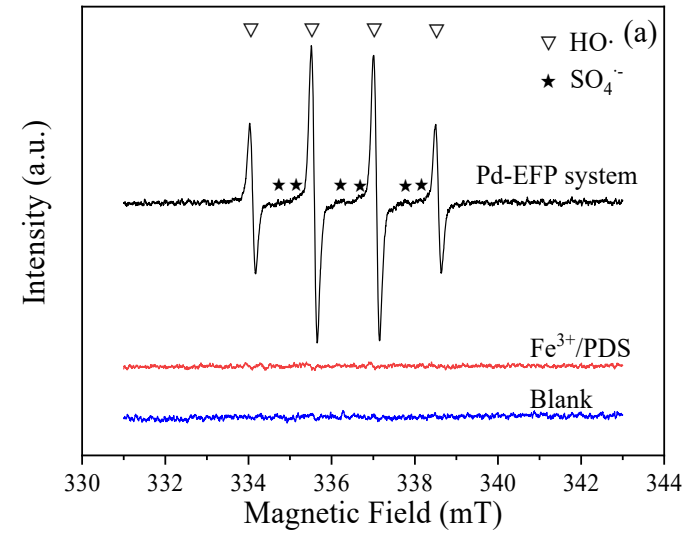

555

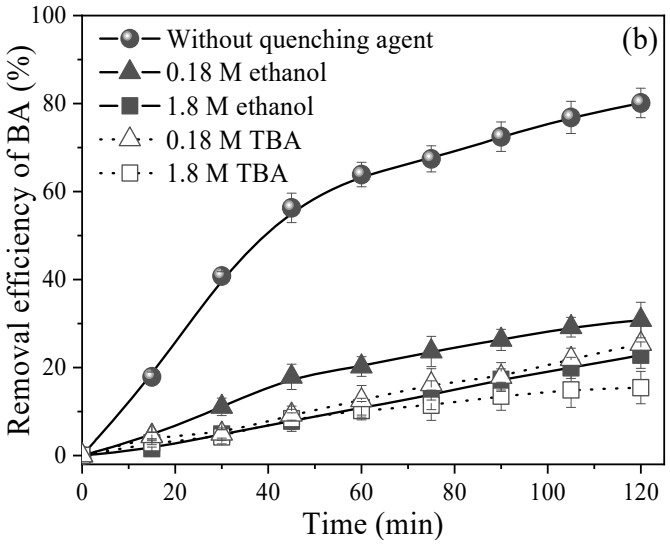

556 **Figure 2.** (a) ESR spectra of DMPO·-OH and DMPO·-SO_4 formed in various systems. (b) Effect

557 of scavengers on the BA degradation in the Pd-EFP system ([BA], 180 μM; [PDS], 10 mM; [Fe^{3+}],

558 36 μM; [Pd/Al_2O_3], 50 mg/120 mL; current density, 3.33 mA/cm^2; initial solution pH, 3.0)

559

560

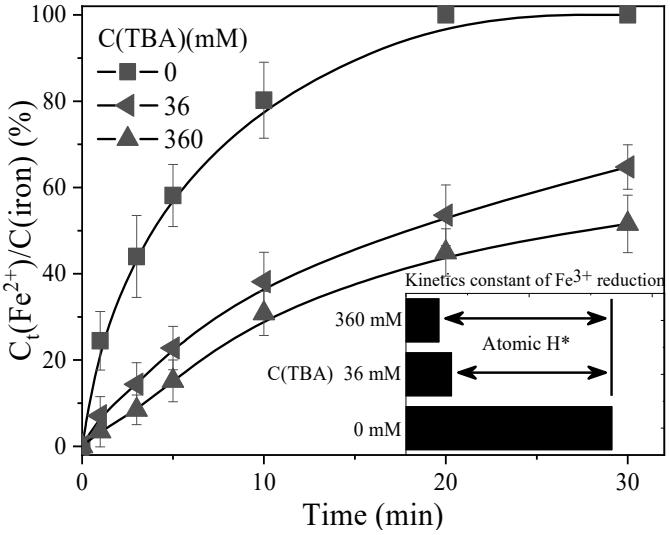

561

562 **Figure 3.** Fe^{2+} concentration variation in the Pd-EFP system without PDS and BA ([Fe^{3+}], 360 μM;

563 [Pd/Al_2O_3], 50 mg/120 mL; current density, 3.33 mA/cm^2; initial solution pH, 3.0)

564

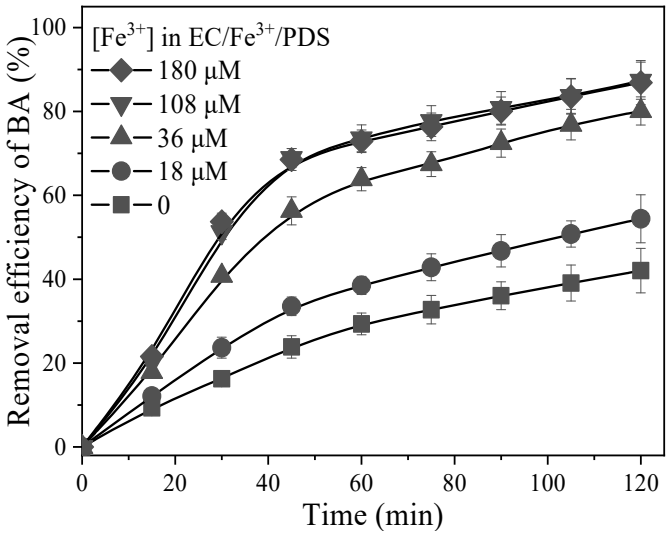

565

566 **Figure 4.** Effect of initial Fe^{3+} addition on the removal efficiency of BA in the Pd-EFP system

567 ([BA], 180 μM; [PDS], 10 mM; [Pd/Al_2O_3], 50 mg/120 mL; current density, 3.33 mA/cm^2; initial

568 solution pH, 3.0)

569

570

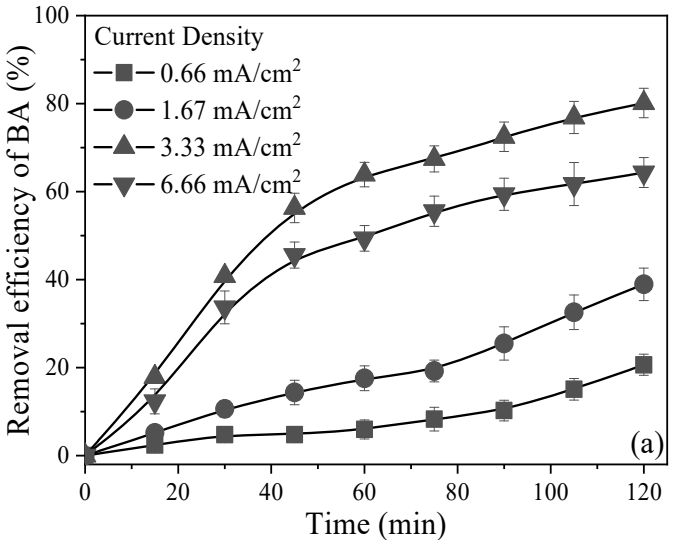

571

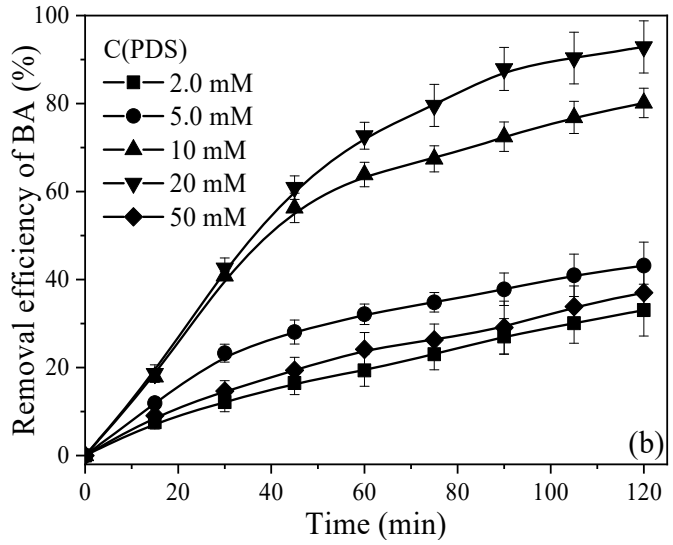

572 **Figure 5.** Effect of current density (a) and initial PDS addition (b) on the removal efficiency of

573 BA in the Pd-EFP system ([BA], 180 μM; [PDS], 10 mM; [Fe^{3+}], 36 μM; [Pd/Al_2O_3], 50 mg/120

574 mL; current density, 3.33 mA/cm^2; initial solution pH, 3.0)

575

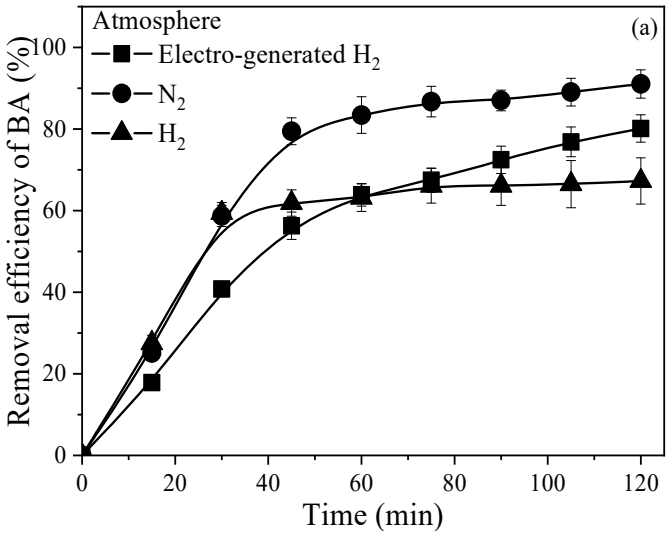

576

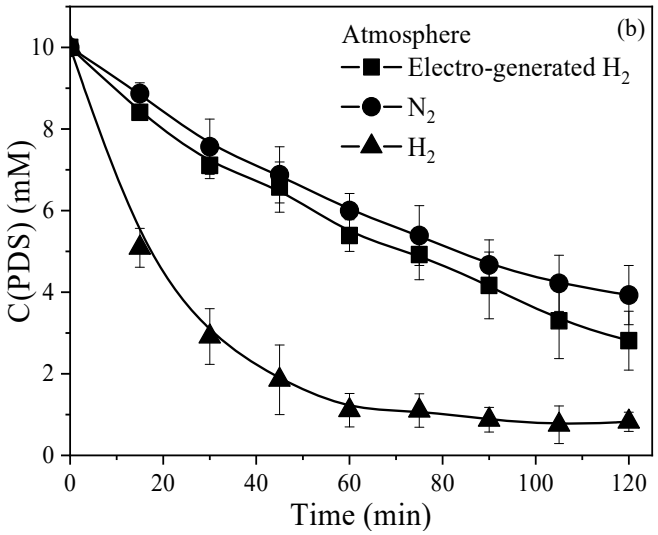

577

578 **Figure 6.** Effect of gas atmosphere in a cathode cell on BA degradation (a) and PDS consumption

579 (b) in the Pd-EFP system ([BA], 180 μM; [PDS], 10 mM; [Fe^{3+}], 36 μM; [Pd/Al_2O_3], 50 mg/120

580 mL; current density, 3.33 mA/cm^2; initial solution pH, 3.0)

581

582

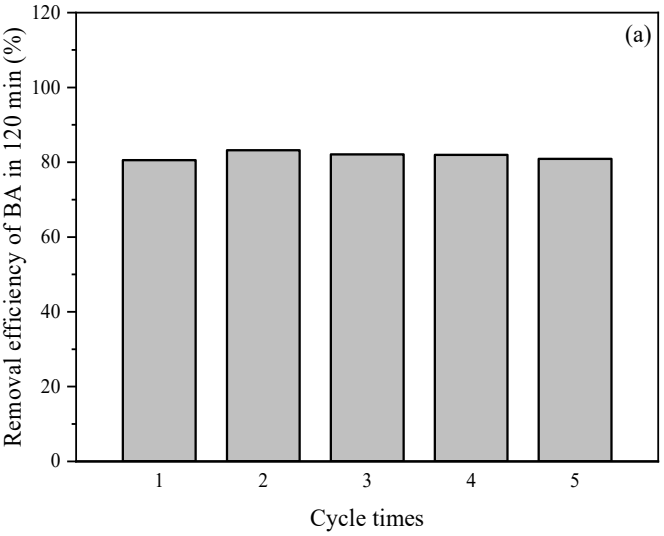

583

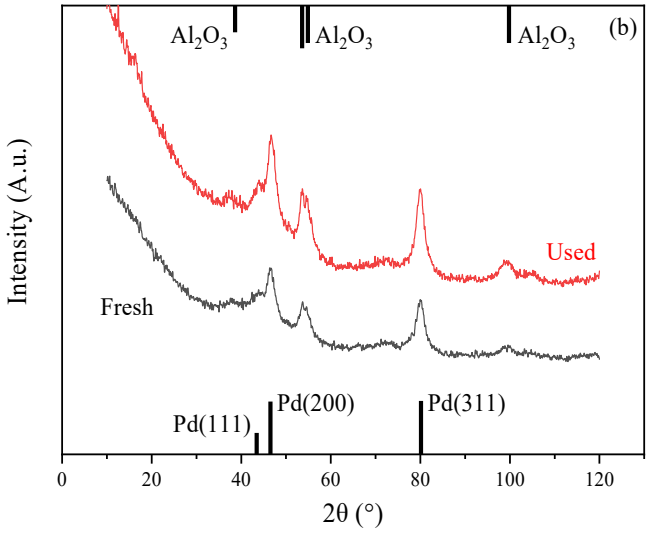

584 **Figure. 7**. (a) The degradation efficiency of BA in the Pd-EFP system for five recycling times

585 ([BA], 180 μM; [PDS], 10 mM; [Fe^{3+}], 36 μM; current density, 3.33 mA/cm^2; initial solution pH,

586 3.0, reaction time, 120 min) (b) XRD spectra of the fresh and used Pd/Al_2O_3 catalysts